Mechanisms for the degradation of phosphor excitation efficiency by short wavelength vacuum ultraviolet radiation in plasma discharge devices

Takeda, Eiji ; Zukawa, Takehiro ; Ishibashi, Tasuku ; Yoshino, Kyohei ; Morita, Yukihiro ; Fujii, Minoru

(Citation)
Journal of Physics and Chemistry of Solids,124:274-280

(Issue Date)
2019-01

(Resource Type)
journal article

(Version)
Accepted Manuscript

(URL)
https://hdl.handle.net/20.500.14094/90008075

Mechanisms for the degradation of phosphor excitation efficiency by short wavelength vacuum ultraviolet radiation in plasma discharge devices

Eiji Takeda[1]

Department of Electric and Electronic Engineering, Graduate School of Engineering, Kobe University, 1-1 Rokkoudai, Nada, Kobe City, Hyogo 657-8501, Japan

Sensing Solution Development Center, Engineering Division, Automotive & Industrial Systems Company, Panasonic Corporation, 1006 Kadoma, Kadoma City, Osaka 571-8506, Japan

Takehiro Zukawa

Institute for Sensors and Devices, Technology Innovation Division, Panasonic Corporation, 1006 Kadoma, Kadoma City, Osaka 571-8508, Japan

Tasuku Ishibashi

Housing Systems Business Division, Eco Solutions Company, Panasonic Corporation, 1048 Kadoma, Kadoma City, Osaka 571-8686, Japan

Kyohei Yoshino

Automotive Infotainment Systems Business Division, Automotive & Industrial Systems Company, Panasonic Corporation, 4261 Ikonobe, Tsuzuki, Yokohama City, Kanagawa 224-8520, Japan

Yukihiro Morita

Institute for Sensors and Devices, Technology Innovation Division, Panasonic Corporation, 1006 Kadoma, Kadoma City, Osaka 571-8508, Japan

Panasonic Device Science Research Alliance Laboratory, Graduate School of Engineering, Osaka University, 1-1 Yamadaoka, Suita City, Osaka 565-0871, Japan

Minoru Fujii

Department of Electric and Electronic Engineering, Graduate School of Engineering, Kobe University, 1-1 Rokkoudai, Nada, Kobe City, Hyogo 657-8501, Japan

[1]Electronic mail: takeda.eiji@jp.panasonic.com

Abstract

The mechanism for the degradation of phosphor excitation efficiency in flat panel plasma discharge devices was investigated. We found that remaining organic compounds contained in the binders of phosphors were transformed to vacuum ultraviolet (VUV) absorbing substances over prolonged aging, which reduce the excitation efficiency of a phosphor, especially in the shorter wavelength VUV range. We also demonstrated that re-deposition of a sputtered protective layer on a phosphor further reduced the luminescence excitation efficiency due to the absorption of VUV radiation by the layer.

Keywords: plasma discharge, luminous degradation, organic residue, protective layer, re-deposition
PACS: 52.75.-d, 79.20.-m, 82.50.-m

1. Introduction

A Xe plasma generated by a dielectric barrier discharge has attracted much attention as a potential mercury-free source of ultraviolet radiation [1, 2, 3]. Numerous Xe plasma light sources have been developed, including cylindrical fluorescent lamps, and flat panel plasma discharge devices such as plasma displays [4, 5, 6], planar lighting fixtures [7, 8, 9] and plate-type virus inactivation units [10, 11, 12]. These devices are alternatives to light emitting diodes (LEDs), which are also effective light sources [13]. Plasma discharge devices have significant size expansion potential and could be fabricated at a reasonable production cost. However, the lifespans of these units are limited to 40,000 to 100,000 hours [1, 5], which are shorter than those of LEDs being usable for over 100,000 hours [14]. Moreover, the luminous efficiency of plasma discharge devices is limited to several tens of lm/W [7], which is inferior to that of LEDs which can generate over 100 lm/W [13, 14]. Therefore, expanding the market for plasma discharge devices requires the increase of the lifespans and luminous efficiency to exceed those of LEDs, which in turn necessitates elucidation of the device degradation mechanisms on luminous efficiency.

In such devices, a protective oxide layer is often formed on the surface of the dielectric layer to protect the electrode and dielectric layer against sputtering during discharge. Electron emission from the surface of this pro-

tective layer actually plays an important role in generating and sustaining the Xe plasma. The vacuum ultraviolet (VUV) light of the Xe plasma excites internal phosphors, and visible or deep ultraviolet light is emitted. Boeuf reported two degradation mechanisms associated with sputtering of the protective layer and damages of the phosphors [5]. In one mechanism, the plasma discharge burns out when the protective layer is eroded out by prolonged sputtering. In the second mechanism, the luminescence quantum efficiency is deteriorated by surface damage of the phosphors induced by both VUV irradiation and ion sputtering. Although many groups have studied these degradation mechanisms and proposed processes to improve the protective layer [15, 16, 17] and phosphors [18, 19, 20], there have been few reports scrutinizing other degradation mechanisms.

In present work, we investigated two mechanisms distinct from those described above. The first one involves loss of luminosity via the adsorption of organic contaminants on the phosphors. VUV radiation can be absorbed by the contaminants to a significant extent. Thus, the absorption of VUV light by organic contaminants can be a factor in luminous degradation. The second mechanism is luminous degradation via the re-deposition of a sputtered protective layer on the phosphors by discharge. Ha *et al.* reported that luminous degradation was suppressed by MgO deposition on phosphors prior to panel sealing due to reduced sputtering damage of the phosphors [21]. However, the same group also reported that the MgO layer on the phosphor affected the luminosity because of the absorption of VUV radiation used for the excitation. The sputtered protective layer generated in the panel as a result of discharge aging is re-deposited on the phosphors located at the other side of the device. Uchidoi also reported that the re-deposition led to a loss of the luminosity of the plasma discharge device because the re-deposition of the sputtered protective layer increases over time [22]. However, detailed quantitative analyses of the relationship between this re-deposition process and luminous degradation have yet to be performed.

The purpose of the present work is to extensively study the two potential degradation mechanisms based on experiments with plasma display panels as model plasma discharge devices. We found that loss of luminance occurred as a result of the absorbance of VUV radiation by organic residues. The consequent formation of byproducts reduces phosphor excitation efficiency by absorbing the shorter wavelength VUV light. Our results also demonstrated that the extent of re-deposition of the sputtered protective layer on the phosphors increased as the device aged, thus reducing the luminance via

the absorption of the shorter wavelength VUV radiation.

2. Experimental Methods

The degradation of plasma discharge devices was assessed using 42 inch high-definition alternating current plasma display panels. A (Mg,Ca)O film with a thickness of 800 nm was deposited on the dielectric layer of the front panel of each experimental unit by electron beam evaporation, so as to form a protective layer. (Mg,Ca)O is the most promising material for protective layers in devices having high Xe concentrations in the discharge gas (so as to achieve both increased VUV radiation generation efficiency and low discharge voltages) because the ion-induced secondary electron emission of this material is greater than that of the more conventional MgO [23, 24, 25, 26]. During the deposition process, the substrate was maintained at 350 °C and O_2 gas was continuously flowed into the chamber at 20 sccm. The evaporation targets used to generate (Mg,Ca)O were sintered mixtures of MgO and CaO. The CaO concentration in the resulting films was experimentally determined to be approximately 9 mol % by X-ray photoelectron spectroscopy (XPS, PHI Quantera SXM, ULVAC PHI). After the (Mg,Ca)O deposition, MgO powder was dispersed on the protective layer to improve the statistical discharge delay [27]. (Y, Gd)BO_3:Eu^{3+} (YGB), a mixture of YBO_3:Tb^{3+} (YBT) and Zn_2SiO_4:Mn^{2+} (ZSM), and $BaMgAl_{10}O_{17}$:Eu^{2+} (BAM) were employed as red, green and blue phosphors on the back panel, respectively. A Ne:Xe mixture was used as the discharge gas, at a pressure in the panel of 450 Torr and a Xe concentration of 20 %. The specifications of the test panels used in this study are shown in Table 1. Panel aging tests were carried out under accelerated conditions, although the aging times reported herein correspond to the actual operational time span. The panels were dismantled and then cut into the pieces at the size of a few cm^2 for the following measurements.

Photoluminescence (PL) measurements in the visible range were carried out by irradiating the back panel samples with VUV light in a vacuum chamber. The pressure in the chamber was approximately 1×10^{-2} Torr and the VUV radiation was provided by the 147 nm line of a Xe excimer lamp (SUS07, USHIO) and the 173 nm line of a Kr excimer lamp (SUS03, USHIO) attached to the chamber. The intensity of the excitation light was adjusted by irradiating $CaCO_3$ powder as a stable reference and monitoring the reflection intensity of the near infrared emission. The PL spectra of various samples were acquired using a grating monochromator together with a photodiode

Table 1: Specifications of the test panels used in this study.

Front Panel	
Bus electrode width	60 μm
Electrode gap	100 μm
Dielectric layer thickness	28 μm
Protective layer thickness	800 nm
Back Panel	
Address electrode width	80 μm
Dielectric layer thickness	10 μm
Barrier rib height	120 μm
Barrier rib width	50 μm
Phosphor thickness	10 μm
Pixel size	675 × 300 μm^2

array coupled to the chamber via an optical fiber. The spectral response of the detection system was calibrated with a standard W lamp reference spectrum.

The amounts of organic residues adsorbed on the samples were determined by thermal desorption spectrometry (TDS, TDS1200, ESCO). Residual gases in the measurement chamber were removed by heating the chamber prior to each measurement. The base pressure prior to each trial was $\sim 1.5 \times 10^{-9}$ Torr and the sample surface temperature was increased at a rate of 10.5 °C/min. The mass of thermally desorbed molecules was identified with a quadrupole mass spectrometer.

The amount of the sputtered protective layer redeposited on the phosphors was estimated by XPS. The samples were excited by a monochromatic X-ray source (Al Kα line at 1486.7 eV), with irradiation at the center of each pixel using a spot size of 100 μm in diameter while monitoring an image of scanning X-ray microscopy (SXM) attached to the XPS chamber. The sample surfaces were neutralized with a combination of electrons and an Ar^+ beam to suppress charging effects during these XPS analyses [28]. The photoelectron signals from the samples were detected at a take-off angle of 45° using a concentric hemispherical analyzer with a pass energy of 69 eV. Y and Mg

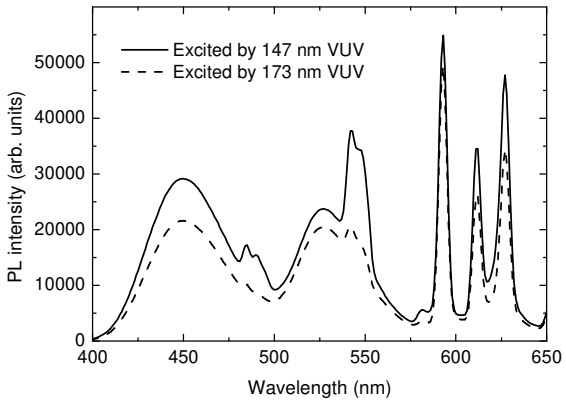

Figure 1: PL spectra acquired from the back panel. The solid and dotted lines correspond to excitation by 147 and 173 nm VUV, respectively.

photoelectron spectra were analyzed to calculate the re-deposition amounts, employing XPS software (MultiPak, ULVAC PHI) to subtract background signals from narrow scan spectra according to the Shirley background [29]. Y and Mg signal intensities were corrected by setting the relative sensitivity factors over the regions being assessed to 171.155 and 17.43 provided by the MultiPak software, respectively.

3. Results and Discussion

3.1. Adsorption of organic compounds on phosphors by VUV irradiation

Figure 1 shows the PL spectra of the back panel sample in response to 147 and 173 nm VUV excitation. The red phosphors generate peaks at 593, 612 and 627 nm, due to the $^5D_0 \rightarrow {}^7F_1$ and $^5D_0 \rightarrow {}^7F_2$ transitions of Eu^{3+} [30]. In the case of the green phosphor, 527 and 543 nm peaks are observed, corresponding to the $^4T_{1s} \rightarrow {}^6A_{1g}$ transition of Mn^{2+} and the $^5D_4 \rightarrow {}^7F_5$ transition of Tb^{3+}, respectively [31]. The 450 nm peak produced by the blue phosphor is caused by the transition from the $4f^6 5d^1$ excited state to the $4f^7$ ground state of Eu^{2+} [30].

Here, we consider the effect of organic residues on the luminous intensity modification of the phosphors. The deposition of organic compounds were

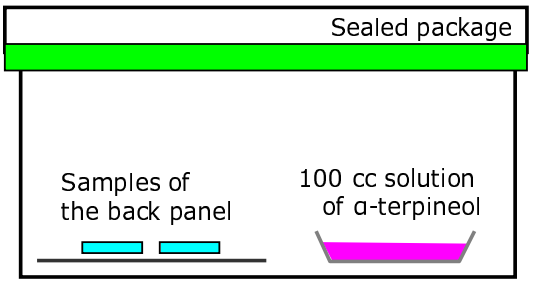

Figure 2: (Color online) Schematic of the apparatus used to expose back panel samples to α-terpineol vapor.

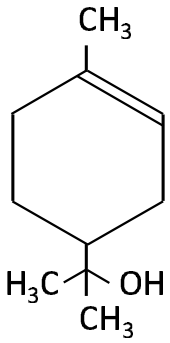

Figure 3: The molecular structure of α-terpineol.

simulated by annealing the back panels in air at 470 °C and exposing the panels in an atmosphere containing α-terpineol (TP) vapor for 2 or 0.5 h (see Figure 2). TP is often used as an organic solvent for the phosphor paste binder, and so can be present as an organic residue in the panels. The structural formula of TP is shown in Figure 3. These test specimens were irradiated with 147 nm VUV light in a vacuum chamber after the exposure to the TP.

Figures 4(a), (b) and (c) summarize the normalized PL intensities at 593, 543 and 450 nm with respect to the initial intensities for the TP-contaminated samples over time in response to continuous irradiation by 147 nm VUV, respectively. The PL intensities of the non-exposed and 0.5 h-exposed samples initially decrease but then recover during 6 h of VUV irradiation. However,

the luminous intensity of the sample exposed for 2 h continually drops, especially at 593 nm. These results suggest that the luminous degradation was not caused by phosphor damage but by organic residues that were modified due to the 147 nm VUV radiation. It should be noted that these experiments were carried out in a vacuum chamber not in a discharge gas atmosphere as found in a plasma discharge device. The luminance recovery described above is therefore attributed to desorption of the organic residues in the vacuum environment, meaning that luminous degradation could occur in an actual panel even in the case of a small amount of organic residue.

The effects of the organic residues on luminous intensity were assessed by following variations in intensity in response to 147 and 173 nm excitation for an untreated sample and samples exposed to TP for 2 h and to 147 nm VUV irradiation for 6 h, as in Figure 5. There is obvious degradation of the luminous intensity in the red wavelength region compared with the green and blue regions in the case of 147 nm excitation. In contrast, 173 nm excitation results in minimal loss of luminance over the entire wavelength range. These results demonstrate that the drop in red luminous intensity solely by 147 nm excitation is not caused by phosphor damage but is rather due to a reduction of 147 nm excitation. This could occur because of the formation of materials absorbing at 147 nm during irradiation of the organic residues.

The VUV irradiation of hydrocarbons tends to generate high molecular weight compounds. As an example, in the case of CH_4, the reaction $n\mathrm{CH_4} + h\nu \rightarrow \mathrm{C}_n\mathrm{H}_{(2n+2)} + (n-1)\mathrm{H_2}$ occurs [32]. This transformation has been shown to increase the absorption of VUV light at shorter wavelengths [33]. Thus, similar reactions are believed to have occurred on the TP-contaminated phosphors used in this study. That is, the TP was transformed to higher molecular weight byproducts during 147 nm VUV irradiation and so the transmittance in the shorter wavelength region decreased. This process in turn degraded the luminous intensity of the phosphors due to decreased excitation efficiency by the 147 nm VUV light.

Figure 6 presents TDS curves acquired from samples of the red, green and blue phosphors annealed in air after the exposure to the TP. During TDS, the loss of fragments of the organic deposits, including $^{16}\mathrm{CH_4}$ (m/z = 16), $^{28}\mathrm{C_2H_4}$ (m/z = 28) and $^{44}\mathrm{C_3H_8}$ (m/z = 44), could be detected. However, since the peaks for these fragments overlap with those generated by H_2O and CO_2 (^{16}O, ^{28}CO and $^{44}\mathrm{CO_2}$), it is difficult to use these peaks to make a conclusive evaluation. Thus, the fragment at m/z =15 ($^{15}\mathrm{CH_3}$) was employed, even though its intensity was relatively weak. It is evident that there was

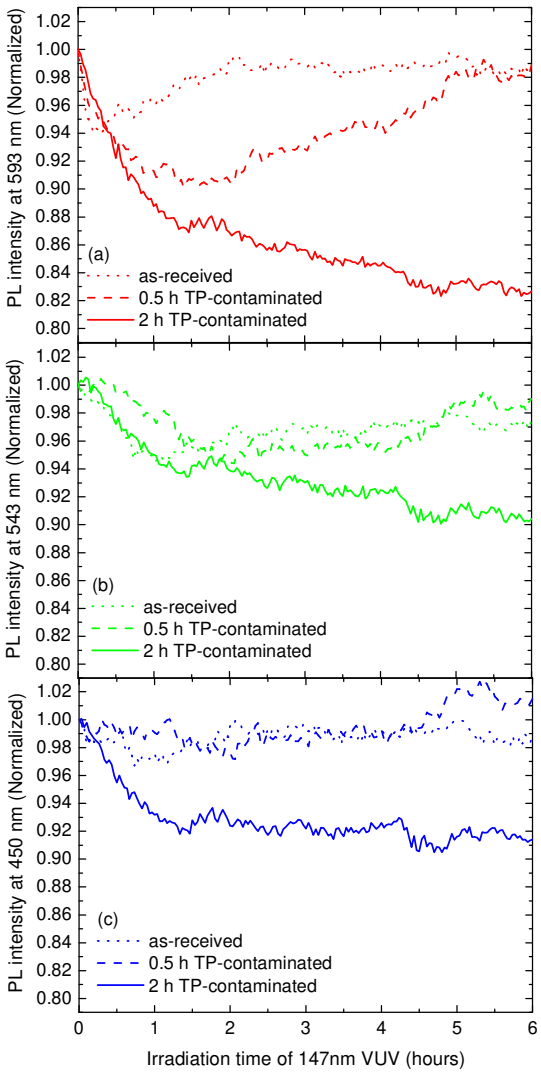

Figure 4: (Color online) Normalized PL intensities at (a) 593, (b) 543 and (c) 450 nm with respect to the initial intensities during continuous irradiation by 147 nm VUV light. Dotted lines correspond to data for as-received samples, while dashed and solid lines indicate data for 0.5 and 2 h TP-contaminated samples, respectively.

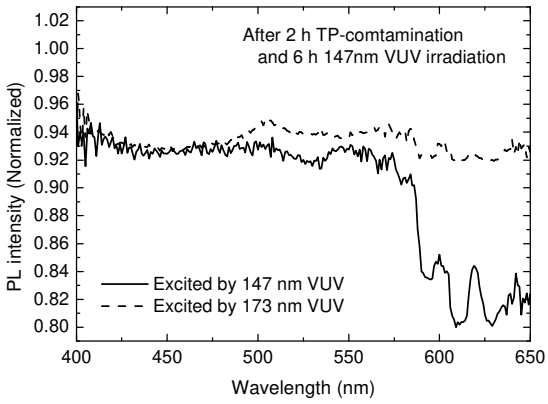

Figure 5: Variations in PL intensities after 2 h exposure to TP and 6 h irradiation with 147 nm VUV light. The solid line corresponds to data for 147 nm VUV excitation, while the dotted line indicates data for 173 nm VUV excitation.

a greater release of organic residues from the red phosphors, indicating that more organic compounds were deposited on these sites. To determine the potential of the physical adsorption on each phosphor, the specific surface area was analyzed using the Brunauer-Emmett-Teller (BET) method, giving values of 2.2, 1.2, 1.4 and 1.7 m^2/g for the YGB, YBT, ZSM and BAM phosphors, respectively. These surface areas are well correlated with the amounts of organic desorption seen in Figure 6. Consequently, the red phosphors are considered to have the largest amount of organic residues because of the widest surface area compared with other phosphors, resulting in reduced 147 nm excitation due to reaction of the organic residues on the red phosphors in response to continuous VUV irradiation.

3.2. Re-deposition of the sputtered protective layer on the phosphors

The test panel was aged for 2200 h and variations in the luminous intensity of the unit were evaluated. Figure 7 shows the relationship between the aging time span and the normalized intensities of red, green blue and white luminance with respect to the initial intensities. As expected, the intensities of all colors decrease with aging. In this trial, the effect of the organic residues described above is excluded because the front and back panels were

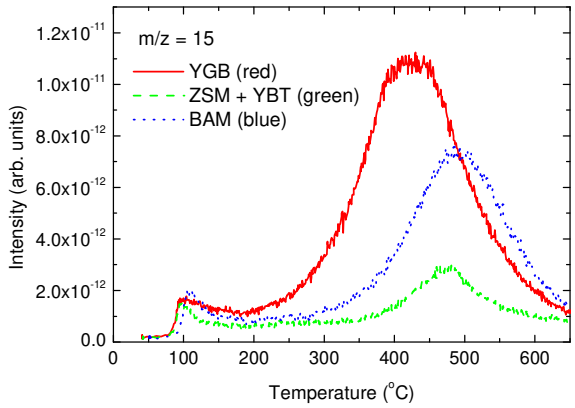

Figure 6: (Color online) TDS curves at m/z = 15 for air-annealed samples of the red, green and blue phosphors.

annealed in air enough to remove them prior to the panel sealing. The red luminance exhibits the lowest degree of degradation because the red phosphor used in the panel is relatively stable, even in response to VUV and plasma irradiation [18]. In addition to the degradation due to phosphor damage, re-deposition of the sputtered (Mg,Ca)O protective layer onto the phosphors degrades the emission efficiency.

The relationship between the loss of panel luminance and the quantity of the (Mg,Ca)O protective layer redeposited on the phosphors during aging was assessed by dismantling panels and analyzing the surfaces of the phosphors on the back panels. Figure 8 shows a SXM image of the back panel sample. By monitoring the SXM image and irradiating the center regions locally in three consecutive pixels with a focused X-ray beam, the red, green and blue pixels could be examined independently in no particular order. Analyzing the elements in these pixels with wide scan measurements enabled the corresponding colors of the pixels to be identified. The results of XPS analyses at red, green and blue pixels on the back panels before and after aging are presented in Figures 9(a), (b) and (c), respectively. Each spectrum is normalized by the peak value of the O 1s photoelectron intensity, which is the most intense within the overall photoelectron kinetic energy range. Here, Mg peaks clearly appear in the spectra, which evidences the re-deposition of

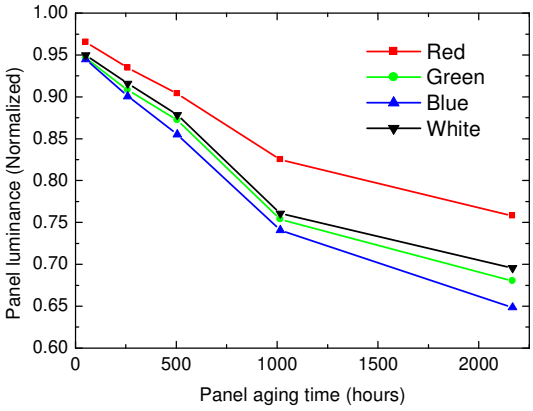

Figure 7: (Color online) Normalized intensities of red, green blue and white luminance upon prolonged aging with respect to the initial intensities.

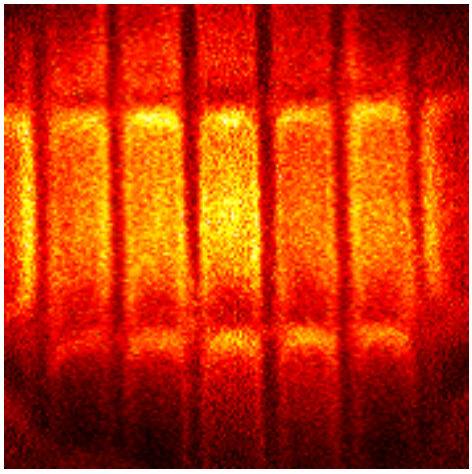

Figure 8: (Color online) Scanning X-ray microscopy image of the back panel sample.

the sputtered (Mg,Ca)O protective layer onto the phosphors after aging.

We subsequently determined the pixel color most suitable for quantifying the re-deposition amounts by XPS analysis. In the case of the blue pixels, it is difficult to quantify the Mg amount because Mg is already present in the

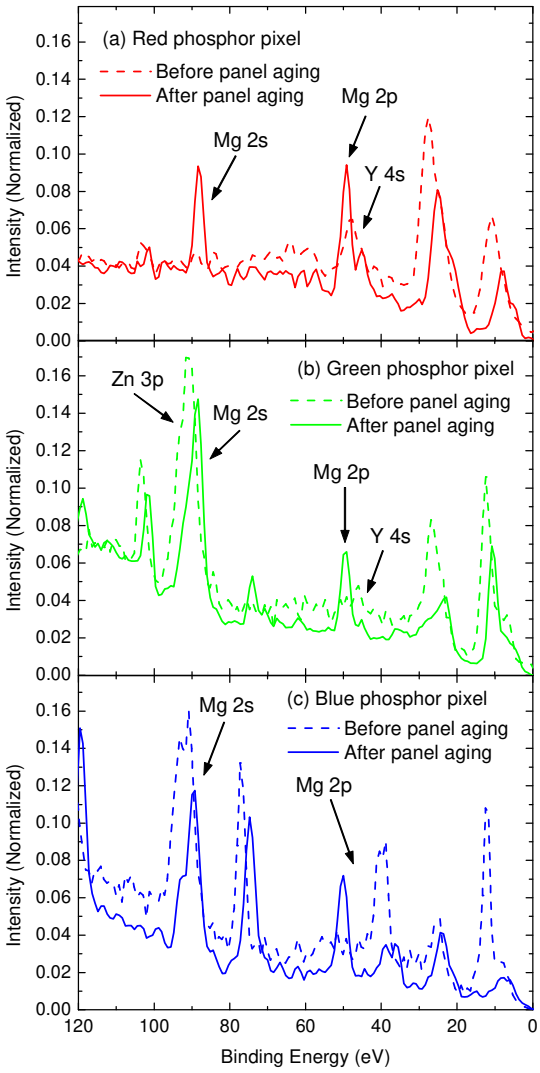

Figure 9: (Color online) X-ray photoelectron spectra acquired from samples of the back panel before and after aging for (a) red, (b) green and (c) blue phosphor pixels. The signal intensity in each spectrum is normalized with respect to the peak value of the O 1s photoelectron intensity.

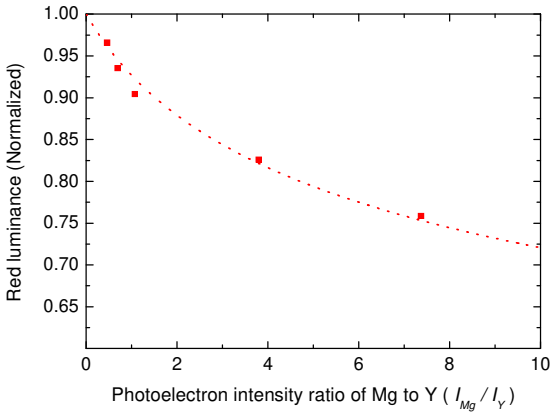

Figure 10: (Color online) Relationship between the normalized red luminance with respect to the initial luminance and the Mg 2s to Y 3d photoelectron intensity ratio. Square data points correspond to experimental data, while the dotted line indicates the results of calculations using Equation 4.

BAM, while in the green pixel spectrum, the Mg 2p and Mg 2s peaks are close to Y 4s and Zn 3p peaks arising from the YBT and ZSM, respectively. The red pixel spectrum contains a Mg 2p peak that is also close to the Y 4s peak generated by the YGB, but the Mg 2s peak is not overlapped. Therefore, we quantified the amounts of Mg in the re-deposition layer by analyzing the Mg 2s peaks produced by the red pixels. The signal intensities from the red phosphors were determined using the Y 3d peak, which is also not obscured by any other peaks.

Determining the peak areas obtained from narrow scans allowed calculation of the ratios of the Mg 2s intensity from the re-deposition layer to the Y 3d intensity of the red phosphor itself (I_{Mg}/I_Y) during aging. Figure 10 plots the normalized red luminance with respect to the initial luminance (L/L_0) as a function of I_{Mg}/I_Y for various panel aging times. It is evident that the luminance decreased as the extent of re-deposition of the (Mg,Ca)O layer onto the red phosphors increased.

Figure 11 presents a schematic diagram showing photoelectron emissions during XPS analyses from the phosphors and the overlapped sputtered (Mg,Ca)O re-deposition layer, where d_R is the thickness of the re-deposition

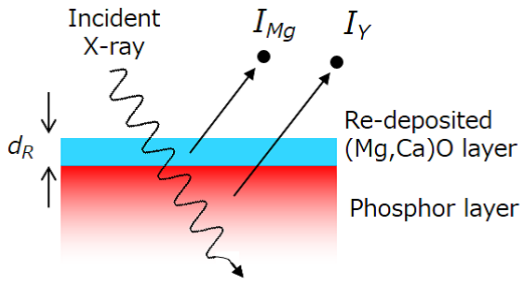

Figure 11: (Color online) Schematic of photoelectron emissions from phosphors and the overlapped re-deposition layer generated by sputtered (Mg,Ca)O during XPS.

layer on the phosphor. In this study, the kinetic energies of the Y 3d and Mg 2s photoelectrons are similar ($\sim$ 1325 and 1395 eV based on Al Kα X-ray excitation with a 1486.7 eV line, respectively). Therefore, if we assume that the attenuation lengths for both Y 3d and Mg 2s photoelectrons moving through the re-deposition layer are equivalent to λ_R, which is the inelastic mean free path (IMFP) of electrons through the re-deposition layer, d_R ($\lesssim$ 8 nm) can be expressed as [34, 35]

$$d_R = \lambda_R \cos\theta \ln\left(\frac{I_Y^{bulk}}{I_{Mg}^{bulk}}\frac{I_{Mg}}{I_Y} + 1\right), \tag{1}$$

where I_Y^{bulk} and I_{Mg}^{bulk} are the signal intensities of Y 3d photoelectrons from the phosphors and Mg 2s photoelectrons from the (Mg,Ca)O layer in the bulk state, respectively, and θ is the detection angle of the photoelectrons with respect to the surface normal ($\theta = 45°$ in this study).

As described above in detail, the PL intensities of our red phosphor samples were degraded only minimally, even by VUV irradiation. Therefore, if we assume that the red luminance is proportional to the VUV excitation intensity and is affected only by modification of the VUV transmission according to changes in d_R, then L/L_0 will follow the Lambert-Beer's law, expressed as [36]

$$\frac{L}{L_0} = \exp\left(-\alpha_R d_R\right) = \exp\left[-\alpha_R \lambda_R \cos\theta \ln\left(\frac{I_Y^{bulk}}{I_{Mg}^{bulk}}\frac{I_{Mg}}{I_Y} + 1\right)\right], \tag{2}$$

where α_R is the VUV absorption coefficient of the re-deposition layer and $I_Y^{bulk}/I_{Mg}^{bulk} = 1.224$ (as obtained by analyzing unaged and aged back panel

samples). The values calculated using Equation 2 are shown in Figure 10 by the dotted line. The calculation results are seen to be in good agreement with the experimental data when the product of the absorption coefficient and IMFP ($\alpha_R \lambda_R$) is set to 0.137.

The IMFP values of Y 3d and Mg 2s photoelectrons passing through a MgO film can be estimated to be approximately 2.8 nm [37]. Therefore, α_R in this study is $\sim 4.89 \times 10^7$ m^{-1} based on $\alpha_R \lambda_R = 0.137$. In plasma discharge devices with Xe discharge gas, the phosphors are excited primarily by VUV lines at 147 and 173 nm [38, 39]. The sharp peak at 147 nm results from the transition from the Xe resonance level Xe*(1s$_4$) to the ground state, while the broad peak at 173 nm arises from the excited molecular dimers $Xe_2{}^*(^1\Sigma_u{}^+)$ and $Xe_2{}^*(^3\Sigma_u{}^+)$ [40]. The adsorption coefficients of bulk MgO at 147 and 173 nm are approximately 4.94×10^7 m^{-1} and 4.64×10^3 m^{-1}, respectively [41]. Thus, the absorption of 147 nm VUV light by the re-deposition layer predominantly contributes to the α_R value cited above. This result indicates that degradation of the panel red luminous intensity can be attributed largely to the degradation of the VUV excitation efficiency of the phosphors due to the absorbance of 147 nm VUV light by the re-deposition layer. The 147 nm to 173 nm emission ratio is also changed upon varying the total pressure or the Xe concentration in the discharge gas [42, 43]. Thus, the α_R value used above is not constant, but can be modified by changes in the discharge gas conditions.

Using Equation 1, the d_R values for panels at various aging times can be calculated, and the relationships between the aging time and the normalized red luminance, and the estimated d_R are graphed in Figures 12(a) and (b), respectively. Figure 12 demonstrates that d_R increases almost in proportion to the aging duration. Evidently, the degradation of the red luminance is correlated with increasing d_R due to decreased VUV excitation efficiency in the shorter wavelength range. In this study, d_R is not increased from zero, but from a threshold thickness of ~ 0.8 nm, which is explained by previous re-deposition during pre-aging prior to the actual aging trials.

4. Conclusions

Mechanisms of the degradation of phosphor excitation efficiency in plasma discharge devices by 147 nm VUV radiation were investigated. We demonstrated that the luminance of the devices was degraded by prolonged VUV irradiation because of the presence of organic residues adsorbed on the phos-

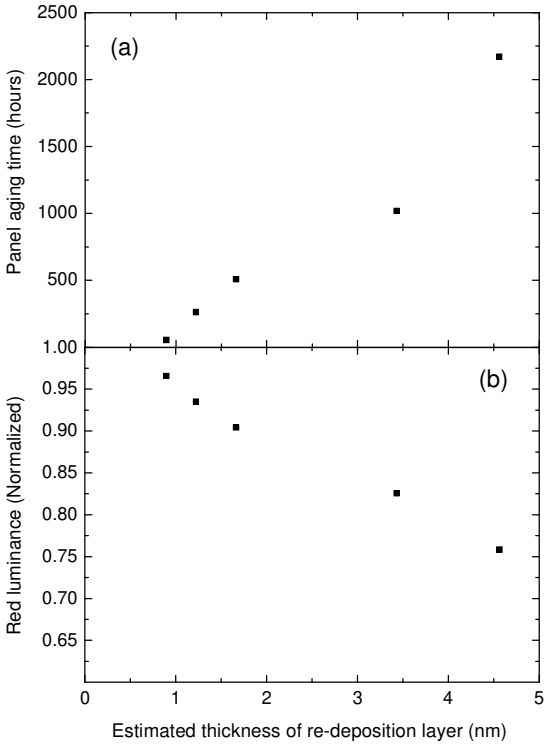

Figure 12: Relationships between (a) the panel aging time and (b) the normalized red luminance, and the estimated thickness of the re-deposition layer.

phors. These results suggest that the organic compounds were converted to substances that absorb VUV light in the shorter wavelength range. XPS analyses indicated that the re-deposition of a sputtered (Mg,Ca)O protective layer on the phosphors increased in proportion to the time period over which the panel was aged. Phosphor excitation was also suppressed by this re-deposition layer since the layer absorbed VUV radiation, especially at shorter wavelengths. Our proposed mechanisms could lead to new approaches to increase the lifespans and luminous efficiency of not only plasma displays but also other plasma discharge devices. This will become evident after applying all possible improvements, such as introducing an annealing process to remove all impurity residues in the panel and controlling the discharge gas

conditions.

Acknowledgments

This work was primarily performed at the facilities of the PDP Advanced Development Group, PDP Devices Business Unit, Visual Products and Display Devices Business Group, AVC Networks Company, Panasonic Corporation. The research was partly supported by the PDP Materials Technology Group, PDP Devices Business Unit, Visual Products and Display Devices Business Group, AVC Networks Company, the AVC Devices Development Center, Technology Planning and Development Center, AVC Networks Company, and the Production Engineering Laboratory, Manufacturing Technology and Engineering Division of the Panasonic Corporation.

References

[1] U. Kogelschatz, Dielectric-barrier Discharges: Their History, Discharge Physics, and Industrial Applications, Plasma Chem. Plasma Process. 23 (2003) 1-46.

[2] B. Jiang, J. Zheng, S. Qiu, M. Wu, Q. Zhang, Z. Yan, Q. Xue, Review on electrical discharge plasma technology for wastewater remediation, Chem. Eng. J. 236 (2014) 348-368.

[3] I. Adamovich, S. D. Baalrud, A. Bogaerts, P. J. Bruggeman, M. Cappelli, V. Colombo, U. Czarnetzki, U. Ebert, J. G. Eden, P. Favia, D. B. Graves, S. Hamaguchi, G. Hieftje, M. Hori, I. D. Kaganovich, U. Kortshagen, M. J. Kushner, N. J. Mason, S. Mazouffre, S. M. Thagard, H.-R. Metelmann, A. Mizuno, E. Moreau, A. B. Murphy, B. A. Niemira, G. S. Oehrlein, Z. Lj Petrovic, L. C. Pitchford, Y.-K. Pu, S. Rauf, O. Sakai, S. Samukawa, S. Starikovskaia, J. Tennyson, K. Terashima, M. M. Turner, M. C. M. van de Sanden, A. Vardelle, The 2017 Plasma Roadmap: Low temperature plasma science and technology, J. Phys. D: Appl. Phys. 50 (2017) 323001-1-46.

[4] H. Uchiike, T. Hirakawa, Color Plasma Displays, Proc. IEEE 90 (2002) 533-539.

[5] J. P. Boeuf, Plasma display panels: physics, recent developments and key issues, J. Phys. D: Appl. Phys. 36 (2003) R53-R79.

[6] L. F. Weber, History of the Plasma Display Panel, IEEE Trans. Plasma Sci. 34 (2006) 268-278.

[7] T. Shiga, L. C. Pitchford, J. P. Boeuf, S. Mikoshiba, Study of efficacy in a mercury-free at discharge fluorescent lamp using a zero-dimensional positive column model, J. Phys. D: Appl. Phys. 36 (2003) 512-521.

[8] K. Awamoto, H. Hirakawa, B. Guo, T. Shinoda, Current Status of the Flexible Surface Light Source Development using LAFi Technology, Proc. 22th Int. Disp. Workshops 1 (2015) 619-620.

[9] S.-J. Park, C. M. Herring, A. E. Mironov, J. H. Cho, J. G. Eden, 25 W of average power at 172 nm in the vacuum ultraviolet from flat,

efficient lamps driven by interlaced arrays of microcavity plasmas, APL Photonics 2 (2017) 041302-1-7.

[10] S. Al-Gharabli, P. Engeβer, D. Gera, S. Klein, T. Oppenländer, Engineering of a highly efficient $Xe_2{}^*$-excilamp (xenon excimer lamp, $\lambda_{max} = 172$ nm, $\eta = 40$ %) and qualitative comparison to a low-pressure mercury lamp (LP-Hg, $\lambda = 185/254$ nm) for water purification, Chemosphere 144 (2016) 811-815.

[11] T. Zukawa, Y. Sasaki, H. Tsujimoto, N. Kamiko, E. Nakamura, Development of a mercury-free plate-type ultraviolet light source, 2016 Int. Ultraviolet Assosi. World Congr. Proc.

[12] R. Prakash, A. M. Hossain, U. N. Pal, N. Kumar, K. Khairnar, M. K. Mohan, Dielectric Barrier Discharge based Mercury-free plasma UV-lamp for efficient water disinfection, Sci. Rep. 7 (2017) 17426-1-8.

[13] C. Hoelen, P. Antonis, D. de Boer, R. Koole, S. Kadijk, Y. Li, Progress in extremely high brightness LED-based light sources, Proc. SPIE 10378 (2017) 103780N-1-19.

[14] M. Schratz, C. Gupta, T. J. Struhs, K. Gray, Reducing energy and maintenance costs while improving light quality and reliability with LED lighting technology, Conf. Rec. 2013 Annu. IEEE Pulp Paper Ind. Tech. Conf. (2013) 43-49.

[15] S. J. Yoon, I. Lee, Theory of the lifetime of the MgO protecting layer in ac plasma display panels, J. Appl. Phys. 91 (2002) 2487-2492.

[16] L. C. Pitchford, J. Wang, D. Piscitelli, J. P. Boeuf, Ion and Neutral Energy Distributions to the MgO Surface and Sputtering Rates in Plasma Display Panel Cells, IEEE Trans. Plasma Sci. 34 (2006) 351-359.

[17] M. El Marsi, R. Moultif, S. Lahlou, S. Rochd, A. Dezairi, Monte Carlo simulations of MgO and $Mg(OH)_2$ thin films sputtering yields by noble-gas ion bombardment in plasma display panel PDP, Nucl. Inst. Methods Phys. Res. B 430 (2018) 72-78.

[18] C. H. Ha, B. Y. Han, J. S. Yoo, H. S. Bae, K.-W. Whang, Characteristics of Phosphor Degradation in AC-Driven Plasma Display Panels, J. Electrochem. Soc. 155 (2008) J230-J234.

[19] K. Sawada, S. Adachi, Unique photoluminescence degradation/recovery phenomena in trivalent ion-activated phosphors, J. Appl. Phys. 118 (2015) 103106-1-7.

[20] L. Amidani, K. Korthout, J. J. Joos, M. van der Linden, H. F. Sijbom, A. Meijerink, D. Poelman, P. F. Smet, P. Glatzel, Oxidation and Luminescence Quenching of Europium in $BaMgAl_{10}O_{17}$ Blue Phosphors, Chem. Mater. 29 (2017) 10122-10129.

[21] C. H. Ha, J. S. Kim, D. C. Jeong, K. W. Whang, The improvement of discharge characteristics and lifetime of alternate current plasma display panel by MgO deposition on the phosphor, J. Appl. Phys. 96 (2004) 4807-4810.

[22] M. Uchidoi, Critical Aspects of the Plasma Display Panel Manufacturing Process, IEEE Trans. Plasma Sci. 34 (2006) 287-293.

[23] T. Zukawa, K. Yoshino, Y. Oe, H. Kawarazaki, K. Aoto, Y. Tanaka, R. Murai, Development of MgCaO Protective Layer of Plasma Display Panels for Decreased Discharge Voltage, SID Int. Symp. Dig. Tech. Pap. 43 (2012) 165-167.

[24] Q. Yan, K. Kotera, H. Zhao, H. Liu, H. Zhou, Y. Tang, X. Deng, Calcium Magnesium Oxide Nano-crystal (Nano-CMO) for Improving Uniformity of High Xe Content PDP, SID Int. Symp. Dig. Tech. Pap. 45 (2014) 208-211.

[25] C.-S. Park, E. Y. Jung, H.-S. Tae, Improvement of luminous efficiency using Li-doped MgO layer coated by MgCaO crystal powders in plasma display panels, Mol. Cryst. Liq. Cryst. 645 (2017) 130-137.

[26] E. Takeda, T. Zukawa, T. Tsujita, K. Yoshino, Y. Morita, Annealing process for recovery of carbonated (Mg,Ca)O protective layer for plasma discharge device, Jpn. J. Appl. Phys. 57 (2018) 096001-1-7.

[27] M. Amatsuchi, A. Hirota, H. Lin, T. Naoi, E. Otani, H. Taniguchi, K. Amemiya, Discharge Time Lag Shortening by Using a New Material Layer in AC PDP, Proc. 12th Int. Disp. Workshops 1 (2005) 435-438.

[28] P. E. Larson, M. A. Kelly, Surface charge neutralization of insulating samples in x-ray photoemission spectroscopy, J. Vac. Sci. Technol. A 16 (1998) 3483-3489.

[29] D. A. Shirley, High-Resolution X-Ray Photoemission Spectrum of the Valence Bands of Gold, Phys. Rev. B 5 (1972) 4709-4714.

[30] R. P. Rao, Phosphors for plasma display panels, in: W. M. Yen, S. Shionoya, H. Yamamoto (Eds.), Phosphor Handbook, second ed., CRC Press, New York, 2006, pp. 745-768.

[31] R. Sato, S. Takeshita, T. Isobe, T. Sawayama, S. Niikura, Photoluminescence Properties of Green-Emitting YBO_3:Ce^{3+},Tb^{3+} Phosphor for near UV Excitation, ECS J. Solid State Sci. Tech. 1 (2012) R163-R168.

[32] A. R. Derk, H. H. Funke, J. L. Falconer, Methane Conversion to Higher Hydrocarbons by UV Irradiation, Ind. Eng. Chem. Res. 47 (2008) 6568-6572.

[33] H. Okabe, D. A. Becker, Vacuum Ultraviolet Photochemistry. VII. Photolysis of *n*-Butane, J. Chem. Phys. 39 (1963) 2549-2555.

[34] M. Seah, L. D. Chiffre, Surface and Interface Characterization, in: H. Czichos, T. Saito, L. Smith (Eds.), Springer Handbook of Materials Measurement Methods, Springer Science+Business Media Inc., Würzburg, 2006, pp. 229-280.

[35] A. Jablonski, Photoelectron emission from thin overlayers, J. Electron Spectrosc. Relat. Phenom. 185 (2012) 498-508.

[36] G. Chartier, Introduction to Optics, Springer Science+Business Media Inc., New York, 2005.

[37] S. Gurban, G. Gergely, J. Toth, D. Varga, A. Jablonski, M. Menyhard, Experimental determination of the inelastic mean free path (IMFP) of electrons in selected oxide films applying surface excitation correction, Surf. Interface Anal. 38 (2006) 624-627.

[38] D. Zhu, L. Song, X. Zhang, H. Kajiyama, Vacuum ultra-violet emission of plasma discharges with high Xe partial pressure using a cathode protective layer with high secondary electron emission, J. Appl. Phys. 115 (2014) 063302-1-7.

[39] H. Loukil, A. Belasri, K. Khodja, Z. Harrache, Theoretical Kinetics Investigation of Xenon Dielectric Barrier Discharge for Excimer Lamp, IEEE Trans. Plasma Sci.42 (2014) 712-720.

[40] Y. Ikeda, J. P. Verboncoeur, P. J. Christenson, C. K. Birdsall, Global modeling of a dielectric barrier discharge in Ne-Xe mixtures for an alternating current plasma display panel, J. Appl. Phys. 86 (1999) 2431-2441.

[41] D. M. Roessler, D. R. Huffman, Magnesium Oxide (MgO), in: E. D. Palik (Eds.), Handbook of Optical Constants of Solids II, Academic Press, Orlando, 1991, pp. 919-955.

[42] J. H. Seo, H. S. Jeong, J. Y. Lee, C. K. Yoon, J. K. Kim, K.-W. Whang, Vacuum ultraviolet emission characteristics from He-Ne-Xe gas discharge in an alternating current plasma display panel cell, J. Appl. Phys. 88 (2000) 1257-1262.

[43] K.-H. Bu, T. H. Shin, B. K. Kim, J. S. Choi, J. D. Kim, Influence of He-Ne-Xe gas composition on vacuum ultraviolet ray spectra in plasma-display panels, J. Soc. Inf. Disp. 10 (2002) 157-162.